Relaxation kinetics of excitons in cuprous oxide

K. E. O'Hara and J. P. Wolfe
Physics Department and Materials Research Laboratory, University of Illinois at Urbana-Champaign, Urbana, Illinois 61801
(Received 12 October 1999; revised manuscript received 15 August 2000)

Due to a simple band structure, the excitons in cuprous oxide (Cu_2O) are a model system for kinetic studies. Cuprous oxide appeared to be a host for a Bose-Einstein condensate of excitons, as the excitons showed transient kinetic energy distributions which matched those expected for a Bose gas near the critical density for Bose-Einstein condensation. However, recent absolute measurements of the exciton density made it clear that two-exciton annihilation is limiting the exciton density to far below the quantum density. This paper reconciles the measured exciton density with the observed exciton energy distributions by using a Boltzmann equation approach. We include experimentally determined rates for acoustic- and optical-phonon emission, conversion between exciton spin states, and two-exciton annihiliation, and use recent diffusion-Monte-Carlo estimates of the exciton-exciton elastic scattering cross section. Many experiments intending to produce a dense exciton gas in Cu_2O used surface photoexcitation, and we found it important to include the resulting spatial inhomogeneities in the model by following the exciton occupation numbers as functions of *space* as well as momentum and time. A detailed but straightforward numerical integration of the resulting Boltzmann equation does in fact match the experimental results, without the assumption of quantum statistics for the excitons.

I. INTRODUCTION

Cuprous oxide is a long-recognized semiconductor that has enjoyed renewed interest during the past two decades due to its perceived promise as a host for a Bose-Einstein condensate of excitons.[1] The excitons in Cu_2O are quite simple. The band edges are at zone center and have only the minimum twofold degeneracy stemming from the electron spin. An electron and a hole bind to form an exciton with the unusually high binding energy of 150 meV. More precisely, 150 meV is the binding energy of the $1s$ exciton; one can observe a complete Rydberg series of hydrogenlike states of the electron and hole.[2,3]

The $1s$ exciton is split by electron-hole exchange into a singlet and triplet. The singlet state, the Γ_2^+ paraexciton, lies 12 meV lower than the triplet Γ_{25}^+ orthoexciton. Radiative recombination of the paraexciton is extremely weak.

The band edges in cuprous oxide both have even parity, so the direct radiative recombination of any $1s$ exciton is dipole-forbidden. The lifetime of a gas of orthoexcitons, in equilibrium at 2 K, against electric-quadrupole radiative recombination is $\sim 10\ \mu$s (Ref. 4). The actual lifetime of the orthoexcitons is limited by their conversion to the paraexciton state, which happens in about 3 ns in a crystal at 2 K. The lifetime of the paraexciton is limited by nonradiative recombination at impurities and defects, and can reach several microseconds in good samples.[5]

There are optical phonons which induce a dipole moment between the bands, making dipole-allowed the recombination of an exciton through simultaneous emission of a photon and optical phonon. This phonon-assisted luminescence is still too slow to affect the exciton population dynamics; the rates are 70/ms for orthoexcitons and 0.14/ms for paraexcitons.[6]

Slow as it is, phonon-assisted luminescence is extremely useful. The optical phonon accepts the difference between the momenta of the recombining exciton and the photon, allowing excitons of any momentum to luminesce with equal probability. The energy of the emitted photon is the total energy of the exciton less that of the optical phonon. The phonon energy is nearly independent of the momentum it was required to accept from the recombining exciton, thanks to the flat dispersion curves of the optical phonons involved.[7] Therefore, the phonon-assisted luminescence spectra reproduce the exciton kinetic energy distribution.

A common experiment uses the green light from an argon-ion laser to produce electron-hole pairs in Cu_2O within 3 μm of the surface. In a crystal at 2 K, these carriers combine to form excitons with a quantum yield near 40%.[6] If the exciton lifetimes remained long at high density, then exciton densities in excess of $10^{20}/\text{cm}^3$ would be readily achievable.

As the bound state of two fermions, excitons should obey Bose statistics. In thermal equilibrium, we expect the occupation number of the exciton kinetic energy eigenstate with energy ε to be given by the Bose-Einstein distribution, $f(\varepsilon)=1/\{\exp[(\varepsilon-\mu)/k_BT]-1\}$, where μ is the chemical potential and T is the temperature of the exciton gas. The Bose statistics of excitons should become noticeable in their equilibrium distribution when the exciton density is sufficiently high that the low-ε occupation numbers become large ($|\mu| \lesssim k_BT$). Based on the density of states for excitons in Cu_2O, the required density is about $10^{17}/\text{cm}^3$ if the exciton gas temperature is 2 K.

Several groups have reported the observation of Bose-shaped distributions of excitons in Cu_2O when using intense pulsed photoexcitation.[8–15] There are, however, several problems with the interpretation of these distributions as quasi-equilibrium Bose distributions. The observed distributions indicate an effective exciton gas temperature higher than that of the lattice, and maintain the characteristic Bose-like (non-Maxwellian) shape for only a few tens of nanoseconds after the laser pulse. We have performed similar experiments un-

der experimental conditions which allowed an estimate of the exciton gas density based on the absolute intensity of the photoluminescence.[16] In our experiments, what appeared to be highly degenerate Bose distributions were observed, but the average exciton densities were 100 times below the densities indicated by fitting the spectra to a Bose distribution.

Experiments indicate a density-dependent annihilation process for the orthoexcitons.[9,11,17] One can envision two such processes: (i) an Auger process in which two excitons collide and one electron-hole pair recombines, giving the band-gap energy to the remaining, ionized, electron and hole; (ii) spin-flip scattering in which two orthoexcitons exchange angular momentum in a collision, becoming two paraexcitons.[18] Of these mechanisms, only Auger decay reduces the net number of excited electron-hole pairs. The processes are readily distinguishable by comparing the relative intensities of orthoexcitons and paraexcitons. In Sec. VI we do so and show that the paraexciton numbers are far too small for spin-flip scattering to be the dominant exciton decay mechanism.

In the experiments, three effects appear at about the same excitation intensity: Auger decay reduces exciton yield, the exciton kinetic energy distribution no longer resembles a Maxwell-Boltzmann distribution, and the apparent exciton gas temperature becomes much higher than that of the lattice (for the common situation of a lattice near 2 K). It is natural to suppose that the resulting Bose-like distributions may be the product of the competition between Auger recombination and cooling by phonon emission. The aim of this paper is to examine this hypothesis in detail.

The following section illustrates this competition by deriving, under a highly simplified model, the steady-state distribution of excitons whose lifetime is too short for them to thermalize. Section III develops a more complete model of the excitons in Cu_2O. Sections IV and V present predictions of this model obtained by using a computer to follow the exciton occupation numbers as a function of time, energy, and spatial position. The model, which ignores the Bose statistics of the excitons, reproduces most of the experimental observations made of excitons in Cu_2O that have thus far been explained only in terms of Bose statistics. In Sec. VI, prior experimental results, including those for resonant excitation, are interpreted in terms of the present calculations.

Our work differs from other treatments[19–21] of the relaxation of excitons in Cu_2O in that it includes *all* of the known kinetic effects, including the motion of photoexcited excitons away from the excitation surface. Previously, Ref. 19 investigated the relaxation of a spatially homogeneous gas of long-lived excitons under the influence of elastic scattering and LA-phonon emission only. Reference 21 added the effects of radiative recombination, but ignored elastic scattering. Reference 20 included the effects of Auger decay (though with a rate 100 times lower than what we have recently measured) and optical-phonon emission, but assumed that the exciton gas was continuously in internal equilibrium, and followed only the density and temperature of the gas. The present calculation uses measured values for all the processes (except elastic scattering, which we estimate from a recent theoretical calculation) and models the geometry of surface photoexcitation so as to allow direct quantitative comparison with experiment.

II. ANALYTIC MODEL FOR THE STEADY-STATE ENERGY DISTRIBUTION

Consider a situation in which excitons are being continuously created with large kinetic energy (above the range of energies observed) and then cooling through acoustic-phonon emission to the extent possible in their finite lifetime. We assume for now that each exciton cools independently of the others, that is, with no elastic collisions to redistribute the energy. For simplicity, we ignore the spin degeneracy of the excitons and assume zero lattice temperature.

The exciton-phonon interaction can be described by an isotropic deformation potential for the excitons, $H=\Xi\nabla\cdot\mathbf{u}$, where $\mathbf{u}$ is the displacement field of the lattice. This interaction, in the limit of vanishing sound velocity, leads to exciton relaxation described by the following differential equation:[22]

$$\frac{\partial g_k}{\partial t}=\frac{\Xi^2 m^2}{\pi\rho\hbar^4}\left(k^2\frac{\partial g_k}{\partial k}+4kg_k\right)-\frac{g_k}{\tau}. \tag{1}$$

Here, $q\equiv|\mathbf{k}-\mathbf{p}|$ denotes the crystal momentum of the phonon emitted, m is the exciton effective mass, which is three times the free electron mass, $\rho=6.1$ g/cm^3 is the density of Cu_2O, and τ is the exciton lifetime. If Auger decay limits the exciton lifetime, then $\tau^{-1}=An$, where $n=(2\pi\hbar)^{-3}\int g_k\,d^3\mathbf{k}$ is the exciton density. We have *omitted* the identical-exciton enhancements—the $(1+g_{\mathbf{k}})$ Bose factors—from Eq. (1) to investigate kinetic effects only, not quantum effects. These factors would have a negligible effect on the kinetics at the exciton densities with which we are concerned.

In applying this theory to the experiments which used excitation pulses longer than one nanosecond, and crystal temperatures near 2 K, we can consider the *driven steady-state* exciton distributions because under the model of Eq. (1) the time required for acoustic phonon cooling to reduce the exciton energy to about 0.2 meV (2 K) is only

$$\frac{\pi\rho\hbar^4}{\Xi^2 m^{5/2}}\frac{1}{\sqrt{0.2\ \text{meV}}}\approx 0.5\ \text{ns}.$$

The steady-state solution to Eq. (1) is

$$g_k=\frac{2\pi^3\rho\hbar^7 n}{\Xi^2 m^2\tau}k^{-4}\exp\left(\frac{-\pi\rho\hbar^4}{\Xi^2 m^2\tau k}\right). \tag{2}$$

The exponential function is close to 1 except at low k, so g_k goes essentially as $1/k^4$.

If the exciton generation rate is sufficient to maintain a density of $n=10^{17}$/cm^3, then Auger decay would limit the exciton lifetime to approximately $\tau=0.1$ ns, given that the Auger decay constant is found to be $A\approx 10^{-16}$ cm^3/ns in recent experiments.[6,16,23] The energy distribution $N(\varepsilon)=(2\pi\hbar)^{-3}\int g_k\,\delta(k^2/2m-\varepsilon)\,d^3\mathbf{k}$ corresponding to the occupation numbers predicted in Eq. (2) is shown in Fig. 1 for the case of $\tau=0.1$ ns. Equation (2) resembles the Bose distribution at low kinetic energies, but its power-law form decreases more slowly than the Bose distribution at high kinetic energies (Fig. 1).

Equation (1) is a very approximate description of exciton relaxation in Cu_2O. Phonon absorption in a lattice at finite

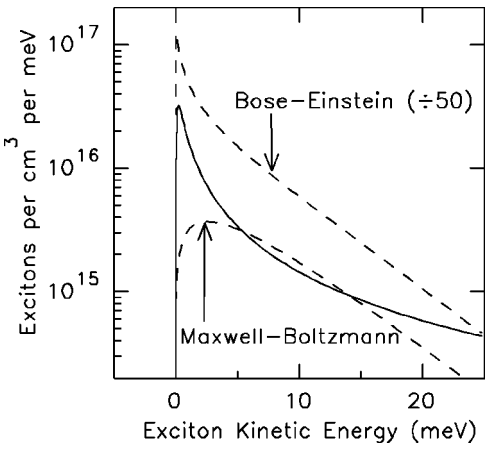

FIG. 1. Solid line: Eq. 2, normalized to $n=10^{17}/\mathrm{cm}^3$. Dashed lines: A nearly saturated Bose-Einstein distribution, and a Maxwell-Boltzmann distribution, both at 60 K.

temperature widens the low-energy peak, to at least the width of a Maxwellian at the lattice temperature (0.3 meV full width at 2 K). Allowing for the finite speed of sound reduces the weight in the low-energy peak, as does inclusion of elastic scattering.

Most experiments use surface photoexcitation, creating an inhomogeneous spatial distribution of excitons. The higher exciton density near the surface causes, through Auger decay, a shorter exciton lifetime, so the excitons near the surface have less time to cool. Generally, one can observe only the superposition of exciton distributions at various depths from the crystal surface. This integrated distribution contains both hot distributions (like that in Fig. 1) from excitons near the surface plus contributions from nearly thermalized excitons further into the crystal, which enhance the low-energy peak. Finally, excitons with kinetic energy greater than that of an optical phonon have the additional cooling mechanism of optical-phonon emission. This tends to straighten out the power-law curve by reducing the occupation numbers of the high-energy states.

This analytical model shows the tendency of the Auger and relaxation processes to produce a long high-energy tail along with a low-energy peak in the kinetic energy distributions. Moreover, the nonequilibrium distribution has positive curvature at high energies, which is consistent with our spectral data (Fig. 7 in Sec. V, for example). A more complete numerical model is developed next.

III. PROCESSES INCLUDED IN THE NUMERICAL MODEL

The Boltzmann equation (Chap. 16 of Ref. 24) describes the evolution of the particle occupation number $g(\mathbf{x},\mathbf{k})$ as a function of both position and particle momentum. For motion free from external forces, the Boltzmann equation has the form

$$\frac{\partial g(\mathbf{x},\mathbf{k})}{\partial t}+\frac{\mathbf{k}\cdot\nabla g(\mathbf{x},\mathbf{k})}{m} = \frac{1}{(2\pi\hbar)^3}\int [W_{\mathbf{p}\to\mathbf{k}}\, g(\mathbf{x},\mathbf{p})-W_{\mathbf{k}\to\mathbf{p}}\, g(\mathbf{x},\mathbf{k})]\, d^3\mathbf{p}.$$

We have *omitted* the $[1+g]$ scattering enhancement factor for bosons because we are investigating ways in which a low-density gas may mimic the spectrum of a degenerate Bose gas. The occupation numbers g were monitored and the ground-state occupation number did not exceed 0.03, except as noted in two exceptional cases presented in Sec. VI.

We can reduce the number of independent variables in $g(\mathbf{x},\mathbf{k})$. The experiments in Sec. V of this paper filled a 50-μm-diam aperture placed on the crystal with pulses of 514.5-nm light from an argon-ion laser, which has an absorption length of about 2.5 μm in Cu_2O. Within the disk, the exciton density depends only on one spatial dimension: depth into the crystal. We can ignore diffusion across the disk within the 10-ns period of interest, but the excitons can diffuse several microns into the crystal within this amount of time. (The exciton diffusivity[25] at 2 K is 60 μm^2/ns.) We store the exciton occupation number $g(z,k,\cos\theta)$ as a function of distance z from the crystal surface, the magnitude k of the exciton momentum, and the angle θ between the exciton momentum and the surface normal.

A. Generation

Above-band-gap excitation produces free electrons and holes, which most likely form excitons in random spin states uniformly distributed in momentum space throughout the first Brillouin zone. We distribute the initially created excitons uniformly throughout a sphere of momentum space corresponding to exciton kinetic energies less than 39 meV. Those excitons initially formed in higher-energy states would emit acoustic and optical phonons at a rate greater than 500/ns, faster than the time scale we need to follow.

B. Acoustic-phonon emission

The three Γ_{25}^{+} orthoexciton states have a strain Hamiltonian of the form[26]

$$H_{\mathrm{ortho}}=\Xi(\epsilon_{xx}+\epsilon_{yy}+\epsilon_{zz})+\begin{vmatrix} \Xi_{zz}(+2\epsilon_{xx}-\epsilon_{yy}-\epsilon_{zz}) & \sqrt{3}\,\Xi_{xy}\epsilon_{xy} & \sqrt{3}\,\Xi_{xy}\epsilon_{xz} \\ \sqrt{3}\,\Xi_{xy}\epsilon_{xy} & \Xi_{zz}(-\epsilon_{xx}+2\epsilon_{yy}-\epsilon_{zz}) & \sqrt{3}\,\Xi_{xy}\epsilon_{yz} \\ \sqrt{3}\,\Xi_{xy}\epsilon_{xz} & \sqrt{3}\,\Xi_{xy}\epsilon_{yz} & \Xi_{zz}(-\epsilon_{xx}-\epsilon_{yy}+2\epsilon_{zz}) \end{vmatrix}$$

in the basis of orthoexcitons states that transforms as $\{yz,xz,xy\}$ under rotations in the cubic group. The paraexciton feels only the isotropic first term. Reimann and Syassen[27] measured the shift in the exciton energies under hydrostatic pressure to determine $\Xi = 1.68$ eV. The shear deformation potentials are best determined from the splitting of the orthoexciton line under shear strain. We obtained $\Xi_{zz} = -0.29$ eV and $\Xi_{xy} = 0.18$ eV by fitting the strain-splitting data of Waters,[28,29] converting the experimentally reported stresses to strains using the elastic compliances in Ref. 30. (Reference 29 does a much more complete analysis to extract the somewhat larger deformation potentials for the holes alone, rather than for the excitons.)

The scattering kernel for longitudinal-acoustic (LA) -phonon scattering by excitons is

$$W_{\mathbf{p}\to\mathbf{k}} = \frac{\pi \Xi^2 |\mathbf{k}-\mathbf{p}|}{\hbar \rho s_L}\left[\delta\left(\frac{p^2}{2m} + s_L|\mathbf{k}-\mathbf{p}| - \frac{k^2}{2m}\right) f_{|\mathbf{k}-\mathbf{p}|} + \delta\left(\frac{p^2}{2m} - s_L|\mathbf{k}-\mathbf{p}| - \frac{k^2}{2m}\right)(1+f_{|\mathbf{k}-\mathbf{p}|})\right],$$

where the f's are phonon occupation numbers and s_L is the speed of longitudinal sound. The phonon occupation numbers are assumed to follow the Planck distribution at the lattice temperature. This means that we neglect any lattice heating or phonon wind effects. This approximation is valid only for excitation densities below about 10^{16} photons per cm^2.

The scattering kernel for transverse acoustic (TA) -phonon emission by orthoexcitons has the same form as that for LA-phonon emission, with the sound velocity s_L replaced by s_T, and with Ξ^2 replaced by the combination of shear deformation potentials $\frac{8}{15}\Xi_{xx}^2 + \frac{1}{2}\Xi yy^2$. The emission of TA phonons is 7% as fast as LA-phonon emission, for orthoexcitons with velocity well above s_L.

C. Optical-phonon emission

Excitons with kinetic energy greater than that of an optical-phonon can cool by optical-phonon emission. There are three optical phonon energies below 40 meV, the eight modes ${}^3\Gamma_{25}^-$, ${}^2\Gamma_{12}^-$, and ${}^3\Gamma_{15}^-$, which we model with one mode at an average energy $E_{\mathrm{op}} = 15$ meV.

Either a deformation potential[31] or Fröhlich interaction[32] results in an optical-phonon emission rate dominated by the number of available final states:

$$W_{\mathbf{p}\to\mathbf{k}} = \frac{8\pi \Xi_{\mathrm{op}}^2 (\mathbf{k}-\mathbf{p})^2}{\hbar \rho E_{\mathrm{op}}}\left[\delta\left(\frac{p^2}{2m} + E_{\mathrm{op}} - \frac{k^2}{2m}\right) f_{\mathrm{op}} + \delta\left(\frac{p^2}{2m} - E_{\mathrm{op}} - \frac{k^2}{2m}\right)(1+f_{\mathrm{op}})\right].$$

The total emission rate of these modes can be estimated from the results of Yu and Shen.[32] For orthoexcitons with 22 meV of kinetic energy, Yu and Shen report that the emission rates γ of various phonons are in the following ratio:

$$\gamma_{\mathrm{LA}} : \gamma_{25}^- : \gamma_{12}^- : \gamma_{15}^- = 1 : 0.14 : 0.18 : 0.21.$$

Therefore, the total optical-phonon emission rate is $0.14 + 0.18 + 0.21 = 0.53$ times the LA-phonon emission rate—for 22-meV orthoexcitons. Setting $\Xi_{\mathrm{op}} = 1.2$ eV in the model reproduces this observed ratio between acoustic- and optical-phonon emission rates.

There is a correction to the deformation potential for phonons with wavelength comparable to the exciton Bohr radius.[33] We make this correction in approximate form by replacing Ξ by $\Xi/[1+(qa_0/4)^2]^2$ in each phonon scattering kernel.

D. Conversion between orthoexcitons and paraexcitons

For interconversion between orthoexcitons and paraexcitons, we develop the acoustic-phonon-emission model suggested in Ref. 34. Conversion from the Γ_{25}^+ orthoexciton to a Γ_2^+ paraexciton requires reorientation of a spin. If the relevant Hamiltonian is assumed to involve the local lattice rotation due to a transverse acoustic phonon, then

$$W_{\mathrm{ortho},\mathbf{p}\to\mathrm{para},\mathbf{k}} = \left[\delta\left(\frac{p^2}{2m} + \Delta - s_L|\mathbf{k}-\mathbf{p}| - \frac{k^2}{2m}\right)(1+f_{|\mathbf{k}-\mathbf{p}|}) + \delta\left(\frac{p^2}{2m} + \Delta + s_L|\mathbf{k}-\mathbf{p}| - \frac{k^2}{2m}\right) f_{|\mathbf{k}-\mathbf{p}|}\right] \times \frac{\pi L^2 |\mathbf{k}-\mathbf{p}|}{\hbar \rho s_T}$$

where $\Delta = 12$ meV is the exchange splitting between orthoexcitons and paraexcitons. The scattering strength $L = 50$ meV is determined from the observed down-conversion rate at 2 K: (0.29 ± 0.03)/ns. The possibility of conversion of orthoexcitons to paraexcitons through collisions is discussed in the concluding section.

E. Auger decay

We take the Auger decay rate to be independent of the relative velocities of the colliding excitons. We follow Ref. 6 in defining the Auger rate constant A so that the rate of Auger decay events per unit volume in a gas of density n is An^2. The rate of change of any exciton occupation number is then

$$\frac{\partial g_{\mathbf{k}}}{\partial t} = -2An g_{\mathbf{k}}$$

because each Auger event destroys *two* excitons, recombining one electron-hole pair and ionizing the other. Estimates of the Auger decay rate within the Bose condensation literature[9,11,17] significantly underestimate the actual rate. We use 10^{-16} cm^3/ns for the Auger constant A, a round figure in the midst of the recent experimental estimates.[6,23,35]

One difficult question is, ''How much of the band-gap energy released in an Auger recombination is deposited in the exciton gas?'' Kavoulakis *et al.*[20] gave this question serious consideration. They argued that the electron and hole liberated by Auger decay shed most of their excess energy into optical phonons. Their argument is based on a comparison of the calculated exciton-electron elastic-scattering cross

section and the rate of emission of Γ_{15}^- optical phonons through the Fröhlich interaction.

In the present model we put all of the excess energy *of the free carriers* into the lattice. We assume that all of the ionized carriers released by Auger decay rebind to form new excitons, and we distribute these excitons in the same way that the initially generated excitons were distributed. Each of the four spin states—three orthoexciton states plus one paraexciton state—receives 1/4 of the newly formed excitons. The complete effect of Auger decay on the exciton occupation numbers is

$$\frac{\partial g_{\mathbf{k}}^{\text{ortho}}}{\partial t} = -2An g_{\mathbf{k}}^{\text{ortho}} + \frac{1}{4}An^2 \times \frac{(2\pi\hbar)^3}{\int d^3\mathbf{p}},$$

$$\frac{\partial g_{\mathbf{k}}^{\text{para}}}{\partial t} = -2An g_{\mathbf{k}}^{\text{para}} + \frac{1}{4}An^2 \times \frac{(2\pi\hbar)^3}{\int d^3\mathbf{p}},$$

where the integrals over $\mathbf{p}$ are over the finite volume of momentum space represented in the computer, and $n = (2\pi\hbar)^{-3}\int [3g_{\mathbf{k}}^{\text{ortho}} + g_{\mathbf{k}}^{\text{para}}]\, d^3\mathbf{p}$ is the total exciton density.

F. Elastic scattering

A recent calculation[36] uses diffusion Monte-Carlo techniques to find the *s*-wave contribution to the elastic-scattering cross section for excitons composed of equal-mass spin-$\frac{1}{2}$ electrons and holes. The results in the low-energy limit are

$$\sigma_{\text{ortho-ortho}} = \begin{cases} 8\pi(3.8a_0)^2, & \Gamma_1 \\ 0, & \Gamma_{15} \\ 8\pi(1.5a_0)^2, & \Gamma_{12} \text{ and } \Gamma_{25}, \end{cases}$$

$$\sigma_{\text{ortho-para}} = 4\pi(0.7a_0)^2,$$

$$\sigma_{\text{para-para}} = 8\pi(2.1a_0)^2.$$

There are three possibilities for collisions between orthoexcitons depending on the relative orientations of their internal angular momenta, labeled by the symmetry designation of the product state of the two orthoexcitons.

In our simulations, we use $\sigma = 50\ \text{nm}^2 \approx 4\pi(2.8a_0)^2$ independent of the spin states of the colliding excitons. The effect of reducing the elastic-scattering cross section to zero is shown in Sec. V.

The contribution of elastic scattering to the Boltzmann equation involves all scatterings from initial momenta $\mathbf{p}$ and $\mathbf{p}_2$ into final momenta $\mathbf{k}$ and $\mathbf{k}_2$:

$$\frac{\partial g(\mathbf{k})}{\partial t} = \frac{2\sigma}{\pi m(2\pi\hbar)^3}\int\int d^3\mathbf{p}_2\, d^3\mathbf{p}\, \delta(p^2 + p_2^2 - k^2 - k_2^2) \times [g(\mathbf{p})g(\mathbf{p}_2) - g(\mathbf{k})g(\mathbf{k}_2)], \quad (3)$$

where $\mathbf{k}_2 = \mathbf{p} + \mathbf{p}_2 - \mathbf{k}$, and σ is assumed independent of $|\mathbf{p} - \mathbf{k}|$. We reduce the collision integral to an integral over the magnitudes of the exciton momenta by replacing $g(\mathbf{p})$, $g(\mathbf{p}_2)$, and $g(\mathbf{k}_2)$ in Eq. (3) by their angular averages g_k, g_{p_2}, and g_{k_2}. Under this approximation,

$$\frac{\partial g(\mathbf{k})}{\partial t} = \frac{8\pi\sigma}{km(2\pi\hbar)^3}\int\int_{p^2+p_2^2>k^2} [g_p g_{p_2} - g(\mathbf{k})g_{k_2}] \times \min(p, p_2, k, k_2)\, p\, dp\, p_2\, dp_2. \quad (4)$$

Physically, the approximation randomizes the directions of those excitons which are going to collide, *before* the collision.

The rate of elastic scattering is $n^2\sigma\overline{\Delta v}$, where $\overline{\Delta v}$ is the relative velocity averaged over all pairs of excitons. With the choices of parameters we have made, there are 3.6 elastic collisions per Auger recombination in a Maxwell-Boltzmann distribution at 2 K.

With our model we find that, during the excitation pulse and near the excitation surface, elastic collisions bring the local exciton distributions close to a Maxwellian shape. Deeper into the crystal and at later times, the local distributions are sufficiently different from Maxwell-Boltzmann distributions to require a full nonequilibrium treatment.

IV. RESULTS FOR SHORT PULSES

Orthoexciton luminescence spectra resulting from high-intensity excitation with sub-nanosecond laser pulses have been thoroughly studied in Ref. 11, which used 100-ps-wide argon-ion laser pulses focused to a diameter of 20 μm, providing a peak incident power density of 10^8 W/cm^2 (3×10^{16} photons/cm^2 per pulse). This would result in 10^{20} photons absorbed per cm^3 near the sample surface. To simulate this experiment, we assume that 30% of the absorbed photons form orthoexcitons and 10% form paraexcitons, consistent with the yield reported in Ref. 6 and a random distribution of spin states. We model the laser pulse as a Gaussian, 100-ps wide at half maximum intensity, producing excitons in a spatial distribution proportional to $\exp(-z/d)$, where $d = 2.5$ μm is the absorption length of the laser light.

Figure 2(a) displays the results of the simulation at various depths z, at the time 200 ps after the center of the generation pulse. Losses to Auger recombination were most severe near the surface where the density was highest. The reduction in the peak density is the reason that the width of the exciton density profiles in Fig. 2(b) is so much greater than the absorption length d. In the $\sim$200 ps between the exciton generation and the sampling time of Fig. 2(b), Auger decay has reduced the exciton density to roughly $(A\times 200\ \text{ps})^{-1} = 5\times10^{16}/\text{cm}^3$. Notice that at this time the density of excitons at the surface is approximately 10^{-3} times the time-integrated density of photons absorbed. Auger decay also makes the mean exciton kinetic energy higher near the excitation surface, as can be seen in Fig. 2(a), by creating new hot excitons.

Surface recombination is not included in this model, but is certainly present in the real system. In order for surface recombination to destroy excitons, excitons must diffuse to the surface. The diffusivity of hot excitons is limited by acoustic-phonon emission to $D = v^2\tau/3 \approx 10$ μm^2/ns (from Fig. 13 later in this paper). The diffusion length for the time shown in Fig. 2 is then $\sqrt{4Dt} \approx 3$ μm so the exciton distribution cannot be seriously affected by surface recombination.

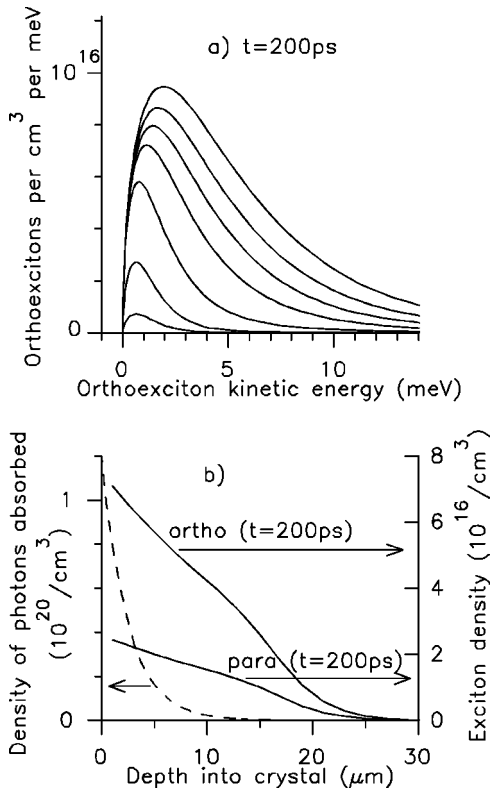

FIG. 2. (a) Simulation results for the energy distribution of orthoexcitons at discrete depths z into the crystal, ranging (top to bottom) from 1 μm to 25 μm in steps of 4 μm. The time is 200 ps after absorption of 3×10^{16} photons per cm^2 from a 100-ps pulse. (b) Dashed curve: generation profile $\exp(-z/d)$ for laser light with an absorption length of 2.5 μm. Solid curves: exciton densities versus depth into the crystal.

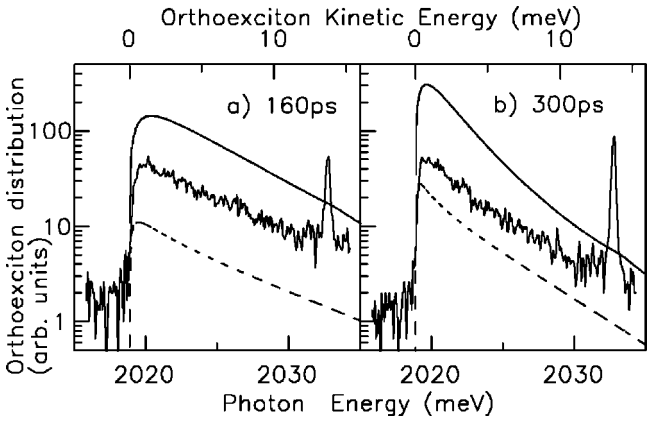

FIG. 3. Our observed orthoexciton luminescence resulting from a focused 150-ps pulse from which at least 10^{15} photons were absorbed per cm^2. Time relative to the center of the pulse is indicated. The luminescence was collected using a microchannel plate photomultiplier with uncalibrated sensitivity, so the vertical axis cannot be converted to an areal density of excitons. Solid curves: the sum over depth z of the simulation results in Fig. 2(a). Dashed curves: fits of the data to Eq. (5). The fitting parameters were (a) $\Theta=73$ K and $\alpha=0.12$, and (b) $\Theta=46$ K and $\alpha=0.08$. The vertical placement of all these curves is arbitrary.

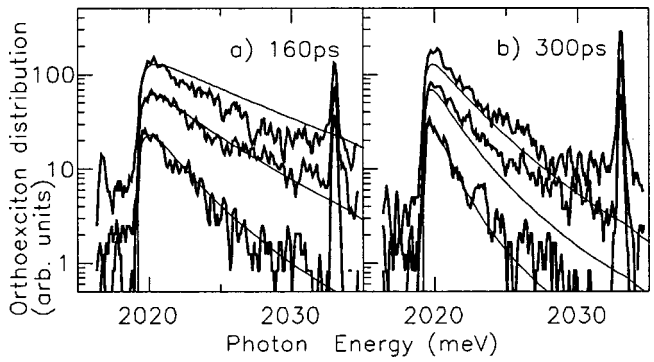

FIG. 4. Observed orthoexciton luminescence spectra corresponding to the excitation conditions of Fig. 3 in Ref. 16. Laser energies are 0.05, 0.5, and 5 nJ in a 180-ps-FWHM pulse. Luminescence is collected from a region much larger than the excitation spot. Thin curves: results of the numerical simulation described in the text. All six simulations are scaled by the same factor.

The observed luminescence is spatially integrated over the inhomogeneous exciton gas. Figure 3 compares the sum of the distributions in Fig. 2(a) with experimental spectra. This experiment of ours was intended to produce conditions similar to those used in Ref. 11. The argon ion laser was focused to a spot which was at most 34 μm wide at half-maximum intensity. Laser pulses containing 12 nJ with a 150-ps width produced a peak incident power of at least 5×10^6 W/cm^2.

Both the experimental and numerical distributions can be reasonably well fit to the *shape* of a Bose distribution:

$$N(\varepsilon)=\frac{a\sqrt{\varepsilon}}{\exp\left(\alpha+\dfrac{\varepsilon}{k_B\Theta}\right)-1}. \tag{5}$$

It is important to note that in these fits the three parameters are allowed to vary independently; the prefactor a is not determined by the exciton density of states as it would be if we were fitting to a real Bose distribution. The parameters obtained from fitting the data are given in the caption to Fig. 3. The best parameters for fitting the *simulation* results in Fig. 3 are less degenerate (have larger α): (a) $\Theta=52$ K and $\alpha=0.63$, and (b) $\Theta=30$ K and $\alpha=0.37$.

In order to compare the model with this experiment at various excitation levels, we must take into account that the effective size of the exciton cloud increases along all three dimensions as the excitation level is increased.[16] Assuming a Gaussian laser spot of diameter D, the exciton-generation profile is $\exp[-8(x^2+y^2)/D^2-z/d]$. We extend the numerical calculations outlined in Sec. III to three spatial dimensions by using $q\equiv z+8d(x^2+y^2)/D^2$ in place of z. The change of variable interferes with our modeling of exciton diffusion, but there is little time for exciton diffusion in these short-pulse experiments, so we ignore exciton diffusion for this case only. Figure 4 compares the model and experimental results for excitation intensities varying over a factor of 100. Agreement is good overall.

Before turning to longer excitation pulses, we mention that if we *do* include the identical-particle enhancements $[1+g]$ to the scattering kernels, the simulation produces results which are visibly indistinguishable from those in Fig. 3.

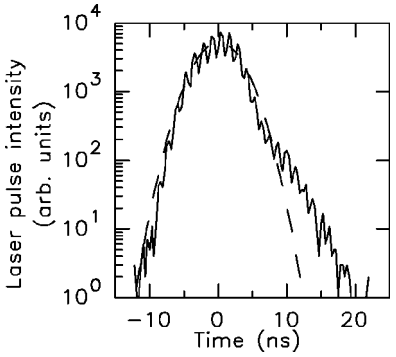

FIG. 5. The cavity-dumped laser pulse shape used to produce the data in this section, measured with the same photon-counting system that collected the exciton luminescence. The trace shown here is not visibly affected by the transit time spread of the photon collection system. The dashed curve is a Gaussian with 7-ns full width.

V. RESULTS FOR LONG PULSES

Experiments using longer (~ 10 ns) laser pulses have produced the orthoexciton spectra that most closely resemble saturated Bose distributions[9] and paraexciton spectra that have been interpreted as a fully saturated Bose distribution, plus a Bose condensate.[12] In our simulations, the longer pulses provide ample time for a fraction of the excitons to cool, so the model predicts quite a sharp low-energy peak in the exciton distributions even during the laser pulse. For the simulation results presented here, we use the Gaussian generation profile with full width at half-maximum intensity equal to 7.0 ns, shown as the dashed line in Fig. 5.

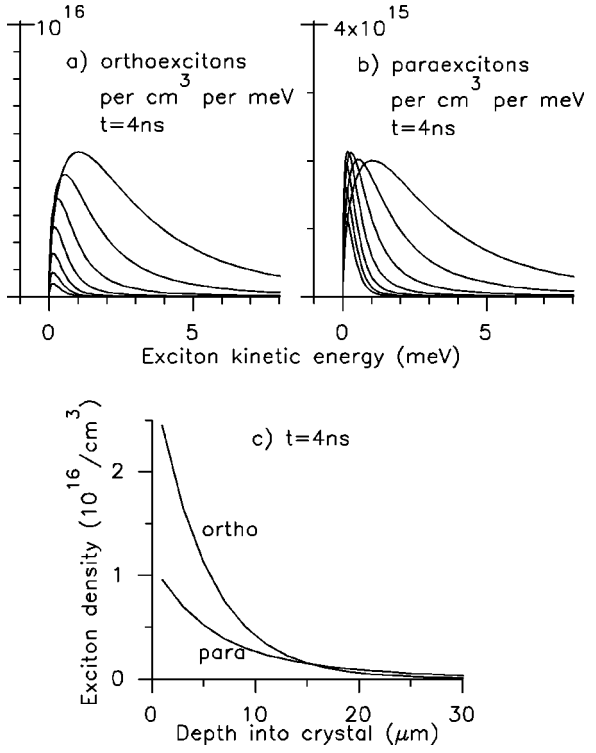

FIG. 6. (a),(b) Simulation results for the energy distribution at depths $z = 1,5,9,13,17,21$, and 25 μm into the crystal. (c) Exciton densities versus depth into the crystal. The time is 4 ns after the creation of 8×10^{14} excitons per cm^2 with a 7-ns pulse.

Figure 6 presents the exciton distributions resulting from the creation of 8×10^{14} excitons per cm^2, chosen to match an experiment in which 2×10^{15} photons were absorbed per cm^2. The excitons were created in an exponential distribution penetrating 2.5 μm deep into the cuprous oxide. The distributions shown are for the time 4 ns after the center of the generation pulse. (The exciton densities are lower than in Fig. 2 because the excitation intensity was ten times higher in that case.)

As we found in the preceding section, the excitons near the surface have a much wider (hotter) energy distribution than those deeper in the crystal. The Auger process in the dense near-surface region is acting to heat the gas locally. The observed exciton distribution is again a sum over this spatial inhomogeneity.

These longer pulses create a situation similar to the driven steady state considered in Sec. II. At the time shown in Fig. 6, the excitation pulse is still creating new hot excitons and driving Auger decay, especially near the excitation surface. Also present are those older excitons that have managed to avoid Auger collisions, and these have had ample time (several nanoseconds) in which to cool to near the lattice temperature.

Exciton diffusion is apparent in the right-hand portion of Fig. 6(c), especially in the paraexcitons. Excitons with velocity near s_L have mean free paths of tens of microns.[25] Moving for 4 ns at the thermal velocity at 2 K, an exciton will have traveled 20 μm by the time shown in Fig. 6.

Surface recombination, which we have not included in the model, certainly reduces the exciton density near the sample surface. Supposing a rather large surface recombination velocity $s\approx10^5$ cm/s and the exciton density in Fig. 6, surface recombination could destroy excitons at a rate $sn\approx3\times10^{12}/(\mathrm{cm}^2\,\mathrm{ns})$. However, surface recombination destroys excitons at a rate linear in the exciton density, while Auger recombination is proportional to density squared, and both are most effective near the excitation surface. Under intense excitation, Auger recombination dominates. In Fig. 6, for example, Auger decay is destroying excitons at a rate of $2\times10^{13}/(\mathrm{cm}^2\,\mathrm{ns})$.

Theory is compared with experiment in Fig. 7. In the experiment, the argon-ion laser pulses filled a 50-μm aperture placed on the sample, providing a well-defined area of uniform excitation. The luminescence was collected using a calibrated photon-counting system. With no adjustment of the parameters, the model predicts an evolving shape of the orthoexciton distribution quite close to what is observed.

The dashed curves are Bose-shaped distributions, Eq. (5), with the two parameters Θ and α adjusted to fit the experiment. If we broaden the curves given by Eq. (5) by the spectrometer resolution function and by the Lorentzian broadening suggested by the direct luminescence line, and replicate the curve for each phonon-assisted luminescence line, then the fit to the data is fairly good at energies up to 2025 meV. (See Fig. 1 in Ref. 16, for example.) The prime difficulty with the explanation of the data in terms of a Bose distribution is that the fit distribution implies large exciton occupation numbers, which in turn imply an exciton density much higher than that indicated by the exciton luminescence intensity. For example, if the shape of the dashed curve in Fig. 7(b) is interpreted as an equilibrium Bose distribution, it im-

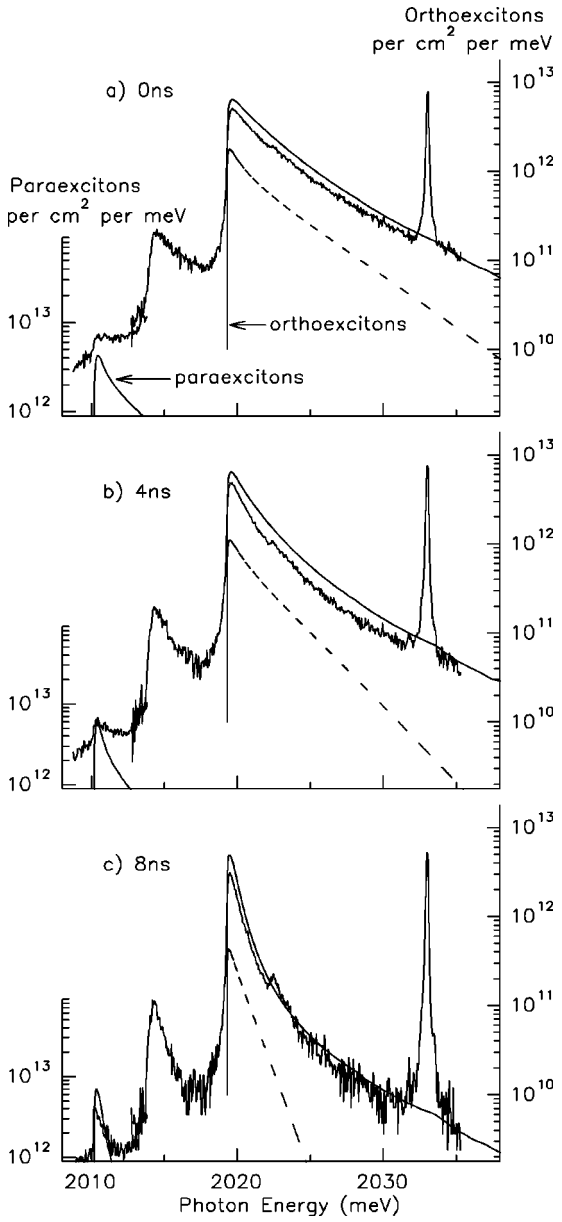

FIG. 7. Luminescence spectra recorded 0, 4, and 8 ns after the center of a 10-ns laser pulse from which the sample absorbed 2×10^{15} photons per cm^2. The right-hand scale is set using the rate for orthoexciton Γ_{12}^--phonon-assisted luminescence and the area of the excited surface from which luminescence was collected. The left-hand scale is set using the rate for paraexciton Γ_{25}^--phonon-assisted luminescence. (The luminescence bands beginning at 2014 and 2023 meV are additional phonon-assisted orthoexciton luminescence replicas.) Solid curves: simulation results assuming the creation of 6×10^{14} orthoexcitons and 2×10^{14} paraexcitons per cm^2 by a Gaussian generation pulse with full width 7 ns. Dashed curves: fits to the Bose shape, Eq. (5), displaced vertically for clarity.

plies a peak exciton density of 10^{19} orthoexcitons per cm^3. If this density holds through a 2-μm layer near the surface, we should see an areal density of excitons of 2×10^{15} orthoexcitons per cm^2, while experimentally we see only 1% of that density. The actual Bose distributions should be 500 times higher than the dashed curves.

The experimental data presented here reveal an important

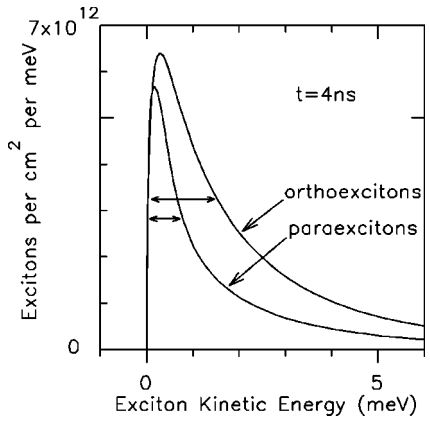

FIG. 8. Simulation results from Fig. 7(b) on a linear scale. The horizontal arrows show full widths at half maxima.

characteristic of the orthoexciton spectrum: at high energies there is a distinctly positive curvature on a semilogarithmic plot. This feature is more apparent in the present data than in earlier publications due to the larger range of energies shown here. The positive curvature is a signature of the nonequilibrium nature of the system as predicted in the analytic theory of Fig. 1 and the simulations in Fig. 7.

Figure 8 compares widths of the orthoexciton and paraexciton distributions given by the same simulation, at the time 4 ns after the center of the laser pulse. The paraexciton distribution is significantly more narrow than the orthoexciton distribution because the paraexcitons are generally older, and thus cooler. The orthoexciton-to-paraexciton conversion rate is 0.3/ns in a crystal at 2 K, so within a 7-ns pulse many of the orthoexcitons have become paraexcitons. Both spin states have their lifetimes shortened by Auger decay, but several microns deep in the crystal, where the density is low, paraexcitons are the more abundant species (see Fig. 6) and these paraexcitons have had several nanoseconds in which to cool.

The actual elastic-scattering cross section for excitons in cuprite might be quite different from the theoretical estimate we used here, so we also present results of a model with *no* elastic scattering between excitons. Comparing Fig. 9 with

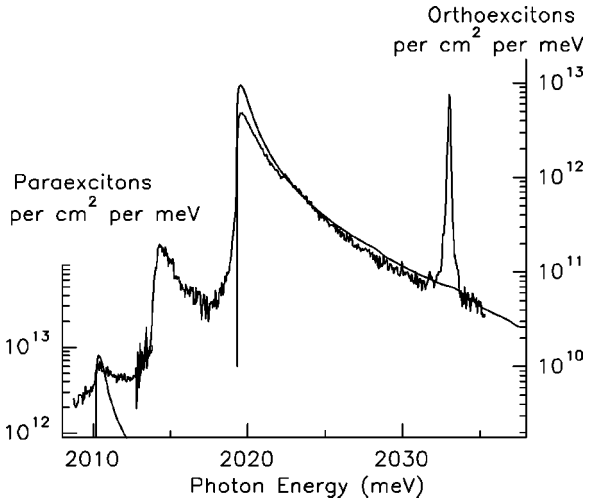

FIG. 9. The luminescence spectrum from Fig. 7(b) compared with a model which includes *no* elastic scattering between excitons.

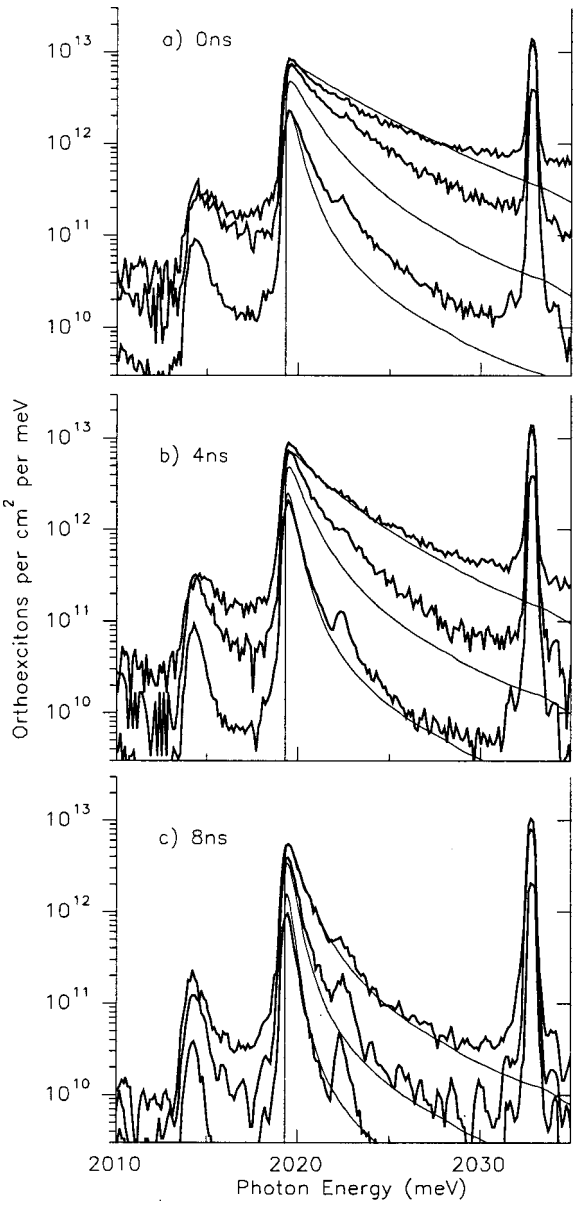

FIG. 10. Luminescence spectra recorded after the sample absorbed 4×10^{13}, 4×10^{14}, and 4×10^{15} photons per cm^2. Thin curves: simulation results appropriate to these excitation levels.

Fig. 7(b), we see that elastic scattering does noticeably even out the nonequilibrium energy distribution. On the other hand, we see that a cross section on the order of 50 nm^2 (enough for three to four elastic collisions per Auger decay collision) does not have a dramatic effect on the energy distributions.

Comparison of model and experiment for a wide range of excitation intensities in Fig. 10 shows good agreement in spectral shapes and agreement within a factor of 2 in intensity—without adjustment of any parameters. The overall agreement gives us confidence in our assertion that the quantum statistics of the exciton gas is not important for understanding the experimental results.

A considerable fraction of the laser pulse energy goes into the lattice, so we must consider the possibility of local lattice heating. We know, however, that the local lattice temperature does cool to near the 2-K bath temperature between laser

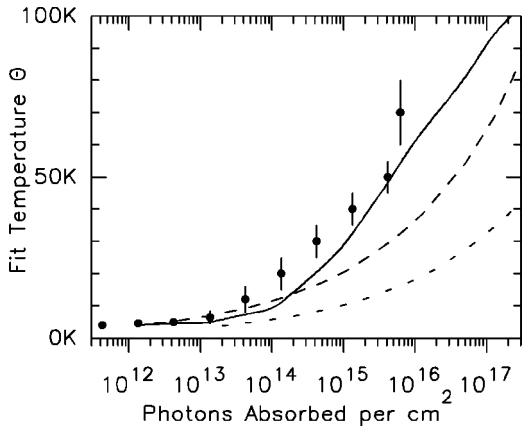

FIG. 11. The maximum apparent temperatures Θ obtained by fitting experimental spectra to Eq. (5). The solid curve is the maximum Θ from fits to the numerical simulations. The broken curves bound the possible local lattice heating by the laser pulse.

pulses, because we have observed orthoexciton distributions below 3 K several tens of nanoseconds after the laser pulse. Thus we need consider only the energy of a single laser pulse.

Suppose all the energy absorbed from each laser pulse is converted directly into lattice heat, with the distribution of heat determined by the optical absorption length. To determine an upper bound to the lattice heating, we ignore diffusion of heat during the tens of nanoseconds of interest. The specific heat of Cu_2O at low temperatures is[37] $c_v\rho=36\,T^3$ J m^{-3} K^{-4} so the local lattice temperature can be found by setting the local density of absorbed energy equal to $\int c_v\rho\,dT=8.9\,T^4$ J m^{-3} K^{-4}. The resulting curve of maximum possible lattice temperature versus laser power appears as the dashed curve in Fig. 11. This curve is certainly an overestimate of the lattice heating because over a 10-ns period ballistic phonons would travel 40 μm, greatly lowering the energy density.

If all phonons left the surface ballistically, the vibrational energy density would correspond to the effective temperatures shown as the dotted curve in Fig. 11. Thus the broken curves give the predicted limits for lattice heating. Obviously the apparent exciton gas temperatures cannot be entirely due to local lattice heating. The numerical model, which ignores lattice heating, cannot be quantitatively accurate at the highest excitation intensities shown. Yet, this model explains most of the apparent exciton gas temperature by inserting at high mean energy the excitons which we assume form from the electrons and holes released in Auger decay events.

To facilitate comparison with earlier work in Cu_2O, we present in Fig. 12 a temperature-density plot of the results of the simulation of a very intense 7-ns excitation pulse. (The simulation created $\sim10^{20}$ excitons per cm^3, integrated over the pulse, near the excitation surface. The instantaneous exciton density is much lower, due to Auger decay during the pulse.) For the exciton distributions at each instant in time, we associate a temperature Θ by fitting the spatially integrated orthoexciton distribution to Eq. (5). For the density we use the maximum local density, that near the excitation surface. The curves marked with dots and circles in Fig. 12 indicate these maximum densities.

We now compare the exciton densities predicted by our

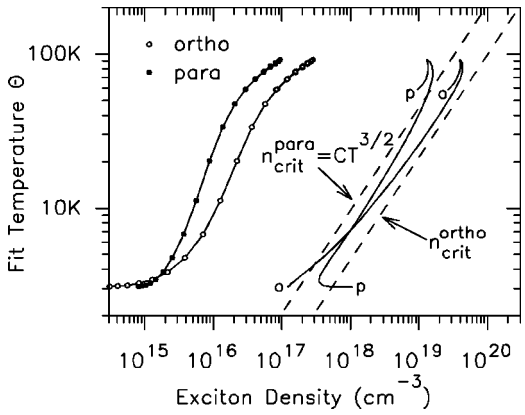

FIG. 12. Traces in density-temperature space for simulation results appropriate for absorption of 10^{17} photons per cm^2 from a 7-ns argon-ion laser pulse. The curves with circles use the fit temperature Θ from Eq. (5) and the local density at the excitation surface. The traces cover times from 6 ns before to 18 ns after the center of the excitation pulse, with one circle every nanosecond. The curves *o-o* and *p-p* use Θ also, but the density is estimated by interpreting the shapes of the spectra as quasiequilibrium Bose distributions. The dashed lines are the critical densities for Bose-Einstein condensation of an ideal gas in equilibrium at temperature Θ.

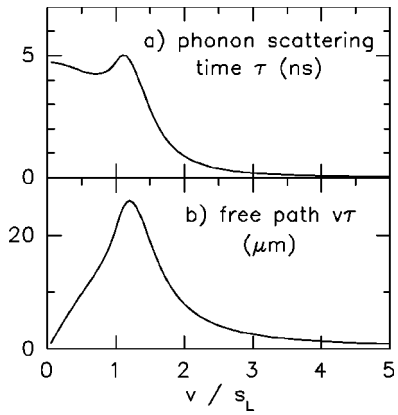

FIG. 13. (a) Mean time before a LA-phonon scattering event as a function of exciton velocity for excitons in Cu_2O at 2 K. (b) The corresponding mean free path.

model (and consistent with luminescence *intensities*) with those derived from fits to the spectral *shapes* alone. That is, we interpret the fit to Eq. (5) as a fit to a quasiequilibrium Bose distribution, and estimate the orthoexciton density through

$$n=\frac{1}{(2\pi\hbar)^3}\int\frac{d^3\mathbf{k}}{\exp\left(\alpha+\frac{\varepsilon}{k_B\Theta}\right)-1}, \tag{6}$$

where $\varepsilon=k^2/2m$. The paraexciton density is estimated by assuming the paraexcitons fill the same volume as the orthoexcitons. Under this assumption, the ratio of densities is the same as the ratio of numbers, which can be determined from the ratio of luminescence intensities. This method was used to analyze experimental spectra[8–15] before the absolute exciton luminescence rates were published. The justification for this procedure was that (a) excellent fits to Bose distributions were obtained, and (b) the exciton densities determined from the Bose fits were consistent with the density of *photons* absorbed (that is, ignoring losses to Auger decay).

The curves *o-o* and *p-p* in Fig. 12 represent the results of this procedure. One would conclude that the orthoexciton density remains very close to the critical density for Bose-Einstein condensation, but never exceeds it. This effect, previously called ''quantum saturation,'' is an artifact of fitting the results of our explicitly *non*-quantum numerical simulation.

VI. DISCUSSION

In this section we consider the experimental evidence for Bose effects in excitons in Cu_2O in light of our present results.

A. Exciton superfluidity?

There have been reports of superfluid transport of excitons after intense above-band-gap photoexcitation. In the first report,[38] the exciton density profiles were measured as a function of depth z from the excitation surface. After intense excitation, the FWHM of these profiles increased linearly with time at a rate greater than s_L.

We have seen that Auger decay can rapidly increase the FWHM of the exciton profile (see Fig. 2) *during and soon after* the excitation pulse. Auger decay does not increase the width of the exciton cloud directly; it decreases the maximum density so that the full width at half-maximum density is larger, mimicking a rapid gas expansion. This effect is short-lived, ending as soon as the density has dropped to the point that Auger decay is no longer the dominant decay mechanism. The model developed in this paper predicts essentially diffusive growth of the exciton cloud beyond 20-μm depth; and thus offers no explanation for the apparently ballistic motion over 100 μm deep into the crystal seen in Ref. 38. The continued rapid expansion may be due to phonon-wind effects.[39]

More recently,[40] excitons have been observed to move across a 2-mm sample at 95% the speed of sound. The excitons were created by 10-ns pulses of doubled YAG laser light, with 10^{17} photons per cm^2, similar to the situation considered for Fig. 12. By 20 ns after the excitation pulse, the exciton density is predicted to be $10^{15}/cm^2$, which is well below the critical density for Bose-Einstein condensation at the 2-K lattice temperature used in Ref. 40. Therefore, we do not expect that quantum statistics is important for these experiments.

Again, phonon-wind effects have been proposed as the mechanism which moves the exciton packet at nearly the speed of sound,[41] an explanation that does not depend on Bose statistics of the excitons. We point out that the exciton mean free path against LA-phonon emission is quite large for excitons moving near the speed of sound (see Fig. 13). Such long mean free paths have been confirmed by measured exciton diffusivities,[25] and may be a large part of the explanation of how these classical exciton packets can travel macroscopic distances in Cu_2O with so little dissipation.

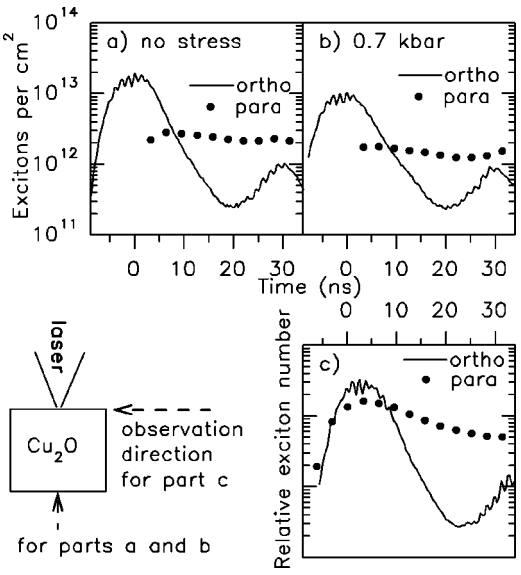

FIG. 14. Observed areal densities of excitons following 7-ns argon-ion laser pulses from which the sample absorbed 10^{16} photons per cm^2. (The peak at 30 ns is due to a secondary laser pulse with about 1% the intensity of the main pulse.) (a) Densities observed by collecting luminescence from the center of the 50-μm aperture used to define the excitation area, with the sample under no stress. (b) Densities observed in the excitation area, in a sample under 0.7 kbar uniaxial compressive stress along [110], based on luminescence collected along [110]. Only the lowest of the three strain-split orthoexciton states is included in the orthoexciton number. (Correction for polarization and anisotropy of the strain-split luminescence lines has been performed.) (c) Relative densities observed by imaging an edge of the Cu_2O sample onto the monochromator, thus collecting edge-scattered luminescence which samples excitons throughout the sample.

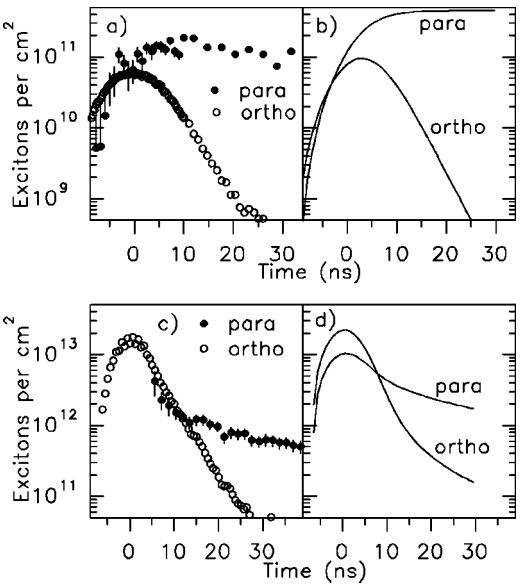

FIG. 15. (a) Observed areal density of excitons resulting from a 10-ns dye laser pulse from which 9×10^{11} 590-nm photons were absorbed per cm^2. (b) Results from our numerical simulation of the experiment of (a), assuming 50% production efficiency for orthoexcitons by 590-nm light (Ref. 6). (c) Experimental results of a 7-ns argon-ion laser pulse from which 2×10^{15} were absorbed per cm^2. (d) Simulation of the experiment of (c), assuming 30% production efficiency for orthoexcitons, and 10% for paraexcitons.

B. Condensed paraexcitons?

There has been a report of Bose-Einstein condensation of paraexcitons in Ref. 12, which used above-band-gap excitation with 10-ns pulses and a uniformly *strained* Cu_2O sample. The principal evidence for Bose-Einstein condensation of paraexcitons was spectra showing paraexciton distributions approximately one-half as wide as the simultaneously observed orthoexciton distributions. A similar ratio of widths, however, is seen in Fig. 8 to follow from the known relaxation processes of an exciton gas well below the quantum density.

The data of Ref. 12 differ from that shown here primarily in the relative numbers of orthoexcitons and paraexcitons observed. Specifically, Ref. 12 reports that the density of paraexcitons greatly exceeds that of orthoexcitons shortly after intense excitation (8×10^{16} photons/cm^2).

Figure 14 presents the results of some of our attempts to reproduce the observations reported in Ref. 12. When uniformly filling an aperture on the crystal surface with the green excitation light, we find results similar to those in Sec. V both with and without stress applied. For Fig. 14(c), we removed the aperture and collected luminescence from the edge of the sample. Edge collection accepts luminescence from the entire volume of the sample. Under these conditions, the relative amount of paraexciton luminescence is greater, but not so great as reported in Ref. 12.

We see from Fig. 14 that determining the ratio of orthoexcitons to paraexcitons from the ratio of their luminescence intensities requires control of the collection geometry and of the shape of the laser spot. In particular, if the excitation pulse has a low-level spatial component outside the main focal spot, the excitons produced in this broader region will not be subject to strong Auger decay. The low-density regions will emphasize paraexciton over orthoexciton luminescence.

Figure 15 shows our present attempt to compare experiment and theory under spatially controlled conditions. Light collection is directly through the sample. The upper parts of Fig. 15 are results for a low-density exciton gas, which in the experiment was created using 590-nm light with an absorption length of 50 μm in Cu_2O. The laser photons in the 10-ns pulse create orthoexcitons, and these orthoexcitons convert into paraexcitons with a decay time of 3 ns. The paraexcitons decay very slowly. The slight decrease in number of visible paraexcitons in Fig. 15 is consistent with diffusion of the excitons out of the observed volume of crystal.

The lower parts of Fig. 15 are for the higher excitation level (2×10^{15} photons absorbed per cm^2) which we have been discussing through most of this section. The fast decay of excitons through Auger decay is obscured by the 7-ns width of the excitation pulse. This situation is closer to a driven steady state, in which the local exciton density n is related to the instantaneous creation rate G of excitons by the laser through $n=\sqrt{G/A}$. The ratio of paraexciton density to orthoexciton density decreases with increasing excitation intensity, as has been reported before.[17]

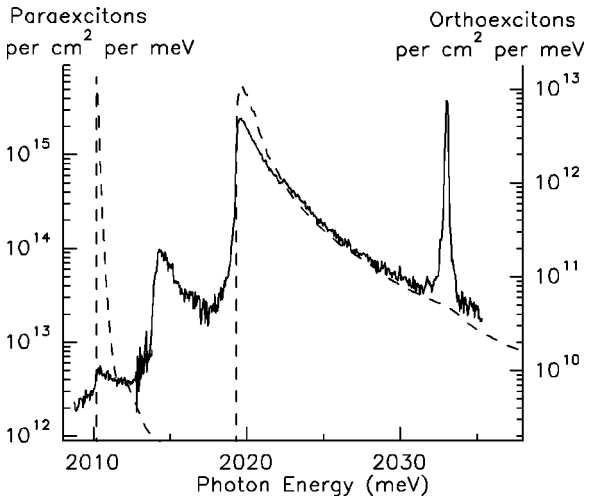

FIG. 16. Luminescence spectrum 4 ns after center of a 10-ns laser pulse from which the sample absorbed 2×10^{15} photons per cm^2. Dashed curves: ortho- and paraexciton luminescence expected if spin-flip collisions were the only interaction between excitons. Under this (unrealistic) assumption, the paraexciton density would be greater than the critical density for Bose-Einstein condensation.

The model predicts excess orthoexcitons at late times in Fig. 15(d). These orthoexcitons are created from the electron-hole pairs liberated from paraexciton Auger decay. Orthoexcitons created in this way have been seen in a confined exciton gas.[42] In this experiment, however, diffusion for 30 ns has spread the paraexcitons beyond the 50-μm-diam excitation area, thus reducing the paraexciton density. The late-time orthoexciton number, proportional to the square of the paraexciton density, is very sensitive to this difference between the experiment and our one-dimensional model.

We have so far assumed that Auger decay of both orthoexcitons and paraexcitons is the principal loss mechanism of these carriers. If instead we assume that the density-dependent orthoexciton decay rate is due to *spin-flip* scattering[18] ($o+o\rightarrow p+p$), the result shown in Fig. 16 is obtained. For this figure only, we have restored the identical-particle enhancement factors in the scattering kernels, because under these assumptions the paraexciton occupation numbers reach 100 at the time shown. We neglected elastic collisions between excitons. The paraexciton intensity which should be expected from the products of spin-flip scattering (dashed line) is far larger than observed in experiment. The Auger mechanism, on the other hand (Fig. 7), accounts reasonably well for both orthoexciton and paraexciton intensities.

C. Nonthermal distributions from resonant excitation

Although the magnitude of Auger decay in Cu_2O prevents a condensate from forming through exciton thermalization, one can put a ''condensate'' in place through resonant excitation. All that is required is a sufficiently strong narrow-band laser source. We put the word ''condensate'' in quotes because the excitons created directly in low-energy states with high occupation numbers are not in equilibrium with, nor have they condensed from, a thermal distribution of excitons.

Recent experiments[14,15] have used two-photon excitation resonant with the orthoexciton electric quadrupole transition. These experiments use surface photoexcitation by 7-ns infrared laser pulses with a quoted energy density near 1 J/cm^2 (Ref. 15). The quoted excitation depth for these conditions is 50 μm (Ref. 14). Defining the two-photon absorption coefficient β by

$$\frac{dI}{dz}=-\beta I^2,$$

where I is the photon flux, we infer that $\beta\approx1$ cm/MW for the conditions used in Refs. 14 and 15. The exciton-generation profile matches the laser absorption profile:

$$G(z,t)=-\frac{1}{2}\frac{dI}{dz}=\frac{1}{2}\frac{\beta[I_0(t)]^2}{[I_0(t)\beta z+1]^2}, \tag{7}$$

where $I_0(t)$ is the photon flux at the sample surface. Note that the effective depth of excitation changes as $I_0(t)$ rises and falls through the laser pulse.

Each orthoexciton is created with momentum equal to that of the pair of photons absorbed, $k/\hbar=3\times10^7$/m. An excitation intensity of 1 J/cm^2 results in the resonant absorption of 10^{21} photons per cm^3 near the excitation surface. Even in the presence of Auger decay, this excitation intensity should produce at least a temporary exciton density on the order of $\sqrt{G/A}\approx10^{17}$/cm^3. This density of excitons, all in states with momentum close to that of the absorbed photons, implies a high occupation number in those states. Despite the high occupation numbers in this scenario, we continue to ignore all the identical-particle scattering enhancements as we apply our numerical model to this type of experiment. (The computed occupation numbers for the zero-momentum state do not exceed 0.16.)

The evidence for effects of Bose statistics in Ref. 15 was that the low-energy peak in the orthoexciton distribution lasted longer in a sample at 2 K than in a sample at 4 K. The argument was that in the warmer crystal, broadening of the resonant absorption line had substantially reduced the two-photon absorption coefficient, resulting in much lower exciton densities.

However, the rate at which orthoexcitons with velocity less than the sound velocity are scattered by phonon absorption is approximately

$$\frac{\Xi^2 m^3 s_L}{4\pi\rho\hbar^4}\frac{16}{\exp(2ms_L^2/k_BT)-1}+\left(\frac{8}{15}\Xi_{zz}^2+\frac{1}{2}\Xi_{xy}^2\right)\frac{m^3 s_T}{4\pi\rho\hbar^4}\frac{16}{\exp(2ms_T^2/k_BT)-1},$$

where the energies $2ms_L^2$ and $2ms_T^2$ (numerically 8 K and 0.8 K) are the approximate energies of the phonons required for energy and momentum conservation. In a 2-K lattice, this rate is 0.4/ns, while in a 4-K lattice it is 2.2/ns. (The fact that low-energy excitons absorb acoustic phonons faster in a 4-K lattice than in a 2-K lattice was confirmed by additional experiments in Ref. 15.)

Figure 17 shows what we would predict for the experiments described in Refs. 14 and 15. Given the intense pulse and short absorption length predicted for the experiment in

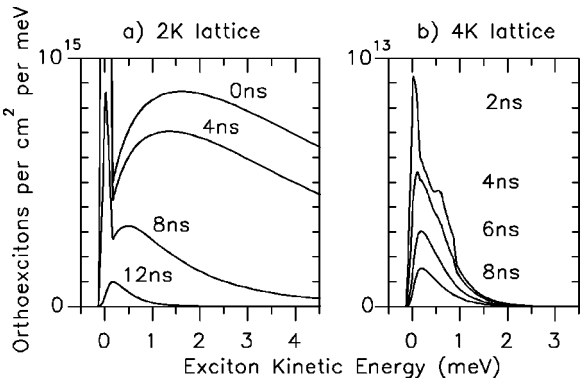

FIG. 17. (a) Numerically predicted orthoexciton distributions at the times indicated relative to the center of a 7-ns-wide pulse $I(t)$ of sufficient intensity to create 3×10^{18} orthoexcitons per cm^2, all with initial energy 0.013 meV in a lattice at 2 K. (b) As (a) but with the orthoexcitons created at very low density in a lattice at 4 K. Note the different selection of times. The distributions have been convoluted with a triangle with FWHM 0.15 meV to match the spectral resolution of Refs. 14 and 15, but the effects of the 15-ns experimental time resolution have *not* been applied here.

the 2-K crystal, our model predicts that Auger decay should produce a very hot gas of excitons. In this case it seems our understanding of the experimental situation is incomplete. However, we note that the hottest observed spectra do resemble our predictions for 8 ns after the pulse center, when the excitation intensity has fallen by a factor of 37.

Note that the peak near zero kinetic energy remains strong despite Auger decay. The spatial inhomogeneity of excitation is important here because toward the end of the laser pulse, the effective absorption profile Eq. (7) extends deep into the crystal. The low-energy peak in the spatially integrated spectrum becomes indistinct about 10 ns after the center of the 7-ns-wide pulse.

To generate Fig. 17(b) for two-photon excitation of a crystal at 4 K we have assumed, following Ref. 15, that the absorption coefficient is greatly reduced. Thus the exciton density is very low and there is no elastic scattering between excitons and no Auger decay. Now only phonon absorption erodes the low-energy peak, but in a 4-K lattice phonon absorption is faster than at 2 K, and the peak disappears in Fig. 17(b) about 4 ns after the center of the excitation pulse. These lifetimes are qualitatively similar to those reported in Ref. 15.

VII. CONCLUSIONS

The discovery that the Auger decay process for excitons in cuprous oxide limits the average exciton density to values well below the quantum density has forced a reinterpretation of the ubiquitous Bose-like energy distributions observed at high excitation densities. Calibrations of the average exciton gas densities revealed that they rarely exceeded 1% of the critical density for Bose-Einstein condensation. In this paper, we have attempted to understand the quantumlike energy distributions as the *nonequilibrium* distributions resulting from known energy-relaxation processes. The principal results can be seen in Fig. 7, which shows the temporal evolution of the energy distribution during and after a 7-ns laser pulse with photon energy above the band gap. A model including Auger recombination, optical- and acoustic-phonon emission, orthoexciton-to-paraexciton conversion, and elastic scattering accounts for the unusual Bose-like distributions remarkably well. Even the intensities of the luminescence spectra are predicted within experimental uncertainty. In addition, the ratio of orthoexciton and paraexciton densities is closely simulated by the model, as shown in Fig. 15. Finally, the observed narrowing of the paraexciton line compared to that of the orthoexcitons is accounted for in the model, as seen in Fig. 8.

A key aspect of this theory is accounting for both the energetics and spatial distributions of the exciton gas. In order to achieve high densities of excitons, near-surface photoexcitation is used. The resulting inhomogeneous excitation profiles are incorporated in the model. We find that the local exciton energy distributions depend strongly on the distance from the crystal surface, and the *sum* of these distributions (corresponding to the optical collection) produces the Bose-like peaks at low energy in the composite spectrum. An apparent fast expansion of the gas within about 20 μm of the crystal surface is predicted (Fig. 2); in fact, the effect is due to fast Auger decay near the surface rather than a rapid transport of excitons. We have not attempted to incorporate phonon-wind effects that could provide a long-lived driving force following the excitation pulse.

For direct comparison to the model calculations, we have employed a well characterized excitation geometry. A 50-μm-diam aperture is pressed against the sample surface and the laser light is adjusted to fill this hole uniformly. We have independently checked the extinction length of the light and have used calibrated optics and electronics to measure the absolute emission strength of the luminescence light, directly gauging the number of excitons emitting per unit area.

Finally, we have applied our theoretical model to recent experiments using *resonant* excitation of excitons. In these cases, calibrated exciton densities are not available, but we have simulated the results for plausible conditions. With intense two-photon excitation, it seems quite possible to create excitons in low-energy states with occupation numbers greatly exceeding unity. Of course, the result is not a thermodynamic condensation, but this seems a fruitful path for observation of quantum effects.

We now realize that a clear imperative for any experimental attempt to form a Bose-Einstein condensate is a quantitative measure of the particle density. This implies regulating the spatial distribution of the excitation, accounting for excitonic diffusion, and measuring the absolute luminescence intensity emitted by the exciton gas. There remains a wealth of information reported in the literature on excitons in cuprous oxide, but interpretations based on a spectroscopic measurement of density are highly questionable. The strong Auger decay process implies that a thermodynamic condensation of excitons in cuprous oxide is far more difficult than previously thought.

ACKNOWLEDGMENTS

The authors thank J. R. Gullingsrud, who developed an alternative Monte-Carlo implementation of this simulation

through its early stages, J. Shumway, who shared his preliminary theoretical results concerning elastic scattering. This work has been supported in part by the National Science Foundation through Grant No. NSF DMR 92-07458 and by the U.S. Department of Energy under Contract No. DEFG02-96ER45439.

[1] *Bose-Einstein Condensation*, edited by A. Griffin, D. W. Snoke, and S. Stringari (Cambridge University Press, Cambridge, 1995), Chaps. 13 and 14.
[2] M. Hayashi and K. Katsuki, J. Phys. Soc. Jpn. **7**, 599 (1952).
[3] J. B. Grun, M. Seiskind, and S. Nikitine, J. Phys. Chem. Solids **19**, 189 (1961).
[4] K. E. O'Hara, Ph.D. thesis, University of Illinois, 1999.
[5] A. Mysyrowicz, D. Hulin, and A. Antonetti, Phys. Rev. Lett. **43**, 1123 (1979).
[6] K. E. O'Hara, J. R. Gullingsrud, and J. P. Wolfe, Phys. Rev. B **60**, 10 872 (1999).
[7] M. M. Beg and S. M. Shapiro, Phys. Rev. B **13**, 1728 (1976).
[8] D. Hulin, A. Mysyrowicz, and C. Benoit á la Guillaume, Phys. Rev. Lett. **45**, 1970 (1980).
[9] D. W. Snoke, J. P. Wolfe, and A. Mysyrowicz, Phys. Rev. Lett. **59**, 827 (1987).
[10] D. W. Snoke, J. P. Wolfe, and A. Mysyrowicz, Phys. Rev. B **41**, 11 171 (1990).
[11] D. W. Snoke and J. P. Wolfe, Phys. Rev. B **42**, 7876 (1990).
[12] Jia Ling Lin and J. P. Wolfe, Phys. Rev. Lett. **71**, 1222 (1993).
[13] N. Naka, S. Kono, M. Hasuo, and N. Nagasawa, Prog. Cryst. Growth Charact. Mater. **33**, 89 (1996).
[14] T. Goto, M. Y. Shen, S. Koyama, and T. Yokuochi, Phys. Rev. B **55**, 7609 (1997); **56**, 4284(E) (1997).
[15] M. Y. Shen, Y. Yokouchi, S. Koyama, and T. Goto, Phys. Rev. B **56**, 13 066 (1997).
[16] K. E. O'Hara, L. C. Ó Súilleabháin, and J. P. Wolfe, Phys. Rev. B **60**, 10 565 (1999).
[17] A. Mysyrowicz, D. Hulin, and C. Benoit á la Guillaume, J. Lumin. **24**, 629 (1981).
[18] G. M. Kavoulakis and A. Mysyrowicz, Phys. Rev. B **61**, 16 619 (2000).
[19] D. W. Snoke and J. P. Wolfe, Phys. Rev. B **39**, 4030 (1989).
[20] G. M. Kavoulakis, Gordon Baym, and J. P. Wolfe, Phys. Rev. B **53**, 7227 (1996).
[21] A. L. Ivanov, C. Ell, and H. Haug, Phys. Status Solidi B **206**, 235 (1998); C. Ell, A. L. Ivanov, and H. Haug, Phys. Rev. B **57**, 9663 (1998).
[22] M. Inoue and E. Hanamua, J. Phys. Soc. Jpn. **41**, 771 (1976).
[23] J. T. Warren, K. E. O'Hara, and J. P. Wolfe, Phys. Rev. B **61**, 8215 (2000).
[24] N. W. Ashcroft and N. D. Mermin, *Solid State Physics* (Harcourt Brace, Fortworth, 1976).
[25] D. P. Trauernicht and J. P. Wolfe, Phys. Rev. B **33**, 8506 (1986).
[26] G. E. Pikus and H. L. Bir, Fiz. Tverd. Tela (Leningrad) **1**, 1642 (1959) [Sov. Phys. Solid State **1**, 1502 (1959)].
[27] K. Riemann and K. Syassen, Phys. Rev. B **39**, 11 113 (1989).
[28] R. G. Waters, F. H. Pollack, R. H. Bruce, and H. Z. Cummins, Phys. Rev. B **21**, 1665 (1980).
[29] H.-R. Trebin, H. Z. Cummins, and J. L. Birman, Phys. Rev. B **23**, 597 (1981).
[30] M. H. Manghani, W. S. Brower, and H. S. Parker, Phys. Status Solidi A **25**, 69 (1974).
[31] D. W. Snoke, D. Braun, and M. Cardona, Phys. Rev. B **44**, 2991 (1991).
[32] P. Y. Yu and Y. R. Shen, Phys. Rev. B **12**, 1377 (1975).
[33] Y. Toyozawa, Prog. Theor. Phys. **20**, 53 (1958).
[34] D. W. Snoke, D. P. Trauernicht, and J. P. Wolfe, Phys. Rev. B **41**, 5266 (1990).
[35] D. W. Snoke and V. Negoita, Phys. Rev. B **61**, 2908 (2000).
[36] J. Shumway and D. M. Ceperley, cond-mat/9907309 (unpublished).
[37] L. V. Gregor, J. Phys. Chem. **66**, 1645 (1962).
[38] D. W. Snoke, J. P. Wolfe, and A. Mysyrowicz, Phys. Rev. Lett. **64**, 2453 (1990).
[39] A. E. Bulatov and S. G. Tikhodeev, Phys. Rev. B **46**, 15 058 (1992).
[40] E. Benson, E. Fortin, and A. Mysyrowicz, Phys. Status Solidi B **191**, 345 (1995); A. Mysyrowicz, E. Benson, and E. Fortin, Phys. Rev. Lett. **77**, 896 (1996); E. Benson, E. Fortin, and A. Mysyrowicz, Solid State Commun. **101**, 313 (1997); E. Benson, E. Fortin, B. Prade, and A. Mysyrowicz, Europhys. Lett. **40**, 311 (1997).
[41] S. G. Tikhodeev, G. A. Kopelevich, and N. A. Gippus, Phys. Status Solidi B **206**, 45 (1998).
[42] D. P. Trauernicht, J. P. Wolfe, and A. Mysyrowicz, Phys. Rev. B **34**, 2561 (1986).